Site NGHP-01-04

By T. Collett, M. Riedel, J. Cochran, R. Boswell, J. Presley, P. Kumar, A. Sathe,
A. Sethi, M. Lall, and the National Gas Hydrate Program Expedition 01 Scientists

Scientific Investigations Report 2012–5054

U.S. Department of the Interior
U.S. Geological Survey

Contents

Figures

Site NGHP-01-04

By T. Collett, M. Riedel, J. Cochran, R. Boswell, J. Presley, P. Kumar, A. Sathe, A. Sethi, M. Lall, and the National Gas Hydrate Program Expedition 01 Scientists

Background and Objectives

Site NGHP-01-04 (Prospectus Site KGGH01) is located at 15° 57.3794' N, 081° 59.4650' E in the central part of the Krishna-Godavari (KG) Basin (fig. 1). The water depth is ~1,081 m. This site was not selected as a primary coring site and only LWD/MWD data were recorded.

The objectives of the work carried out at this site follow the general objectives of NGHP Expedition 01, with a focus on the LWD/MWD operations only:

- Study the occurrence of gas hydrate and establish the background geophysical baselines for gas-hydrate studies;
- Define the relationship between the sedimentology and structure of the sediments and the occurrence and concentration of gas hydrate;
- Calibrate remote sensing data such as seismic data by acquiring LWD/MWD data.

Site NGHP-01-04 is located just E of seismic line AD-94-25 within a well-developed slope-basin (figs. 2 and 3). A clear BSR is present along most of the line. Between shot points 275 and 350 it cross-cuts the sedimentary layers, but for remainder of the line it occurs as reflections parallel to the basin fill. At Site NGHP-01-04, the BSR is at a depth of ~182 mbsf but it becomes shallower towards the NW in response to decreasing seafloor depth. The BSR also abruptly ends in the SE part of the seismic line at shot point 550 where it intersects with a deep-rooted fault that can be traced from almost the seafloor to 2.3 s TWT. No strong reflections indicating the presence of free gas below the BSR are identified on seismic line AD-94-25 within a kilometer of the drill site; thus drilling/coring operations were planned to a total depth of 300 mbsf.

Operations

This operations summary covers the transit from Site NGHP-01-03 (GDDH05-A) to Site NGHP-01-04 (KGGH01-A) and LWD/MWD drilling operations in Hole NGHP-01-04A (fig. 4). Schedule details and statistics for this site can be found as Appendixes:

- Appendix 1: NGHP Expedition 01 Operations Schedules
- Appendix 2: NGHP Expedition 01 Operations Statistics

Included in the Glossary is a list of standard or commonly used operations terms and acronyms.

Hole NGHP-01-04A

The 6.5 NMI transit from Site NGHP-01-03 to Site NGHP-01-04 was completed in 1.25 hours at an average speed of 5.3 knots.

The first and only hole of Site NGHP-01-04 was drilled on Leg 2 of NGHP Expedition 01 as the fourth hole of a twelve-hole LWD/MWD transect. The sea voyage ended at 1112 hr on May 23, 2006; thrusters/hydrophones were immediately lowered. The vessel was switched from cruise mode to DP control at 1130 hr and at 1159 hr a positioning beacon was deployed at the Hole NGHP-01-04A location coordinates. The LWD/MWD tools, consisting of the GeoVISION (RAB), EcoScope, SonicVISION, and TeleScope, were assembled. The ProVISION NMR tool was not deployed in this hole. Once assembled, the LWD tools were flow tested, the nuclear source was loaded, and the drill string was lowered to the seafloor. The drill string was spaced out for spudding and a tag of the seafloor indicated a mudline depth of 1092.0 mbrf. For reference, the PDR depth at this site, adjusted to the rig floor DES, was 1092.4 mbrf. Hole NGHP-01-04A was spudded at 1610 hr on May 23. LWD/MWD drilling continued at a controlled rate of 21.1 m/h (or 17.1 m average net ROP including connection time) to a total depth of 300.0 mbsf. The hole was displaced with 92 barrels of 10.5 ppg mud, the top drive was set back, and the drill string was pulled clear of the seafloor at 1130 hr on 24 May. After removing the nuclear source and downloading data, the LWD/MWD BHA was racked back in the derrick. The rig was secured for transit, the beacon recovered, and the vessel was underway for Site NGHP-01-05 (KGGH02-A) at 1445 hr. This completed operations at Site NGHP-01-04.

Downhole Logging

Logging While Drilling

Operations

After tagging the seafloor at 1,092 mbrf (driller's depth), Hole NGHP-01-04A was spudded at 1610 hr on May 23, 2006, local time. LWD tools in the BHA included the GeoVISION resistivity, the EcoScope, the SonicVISION, and the TeleScope MWD. For details on each LWD tool and the measurements it makes, see the "Downhole Logging" section in the "Methods" chapter.

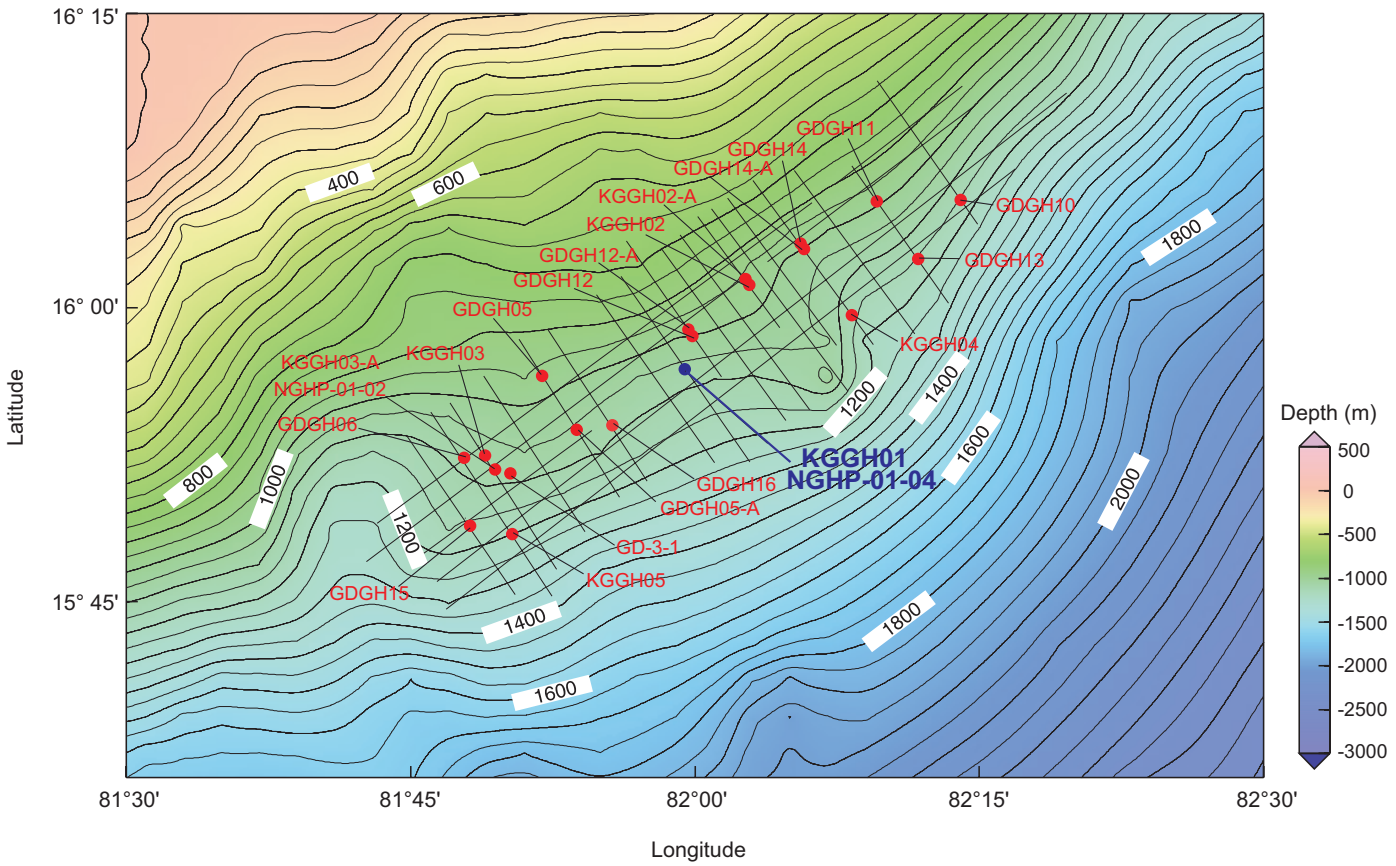

Figure 1. Location of Site NGHP-01-04 (Prospectus Site KGGH01) in the Krishna-Godavari (KG) Basin.

To avoid washing out the hole near the seafloor, Hole NGHP-01-04A was spudded at a relatively low flow rate. The first 10 m were drilled at 100 gpm with a rotation rate of 10 rpm and a rate of penetration (ROP) of 25 m/h. Below 10 mbsf, the rotation rate was increased to 30 rpm; over the range of 30–35 mbsf, the rotation rate was increased to 60 rpm and the flow rate was increased to ~370 gpm until the LWD tools turned on, continuing to drill with a ROP of 25 m/h. The target depth of 300 mbsf (1,392 mbrf) was reached at 0945 hr on May 24, 2006. After pulling the tool string to the surface, data download and rig down were completed at 1430 hr on May 24. (The depths in mbsf mentioned above are referenced to the seafloor depth tagged by the driller.)

Gas Monitoring with Real Time LWD/MWD Data

The LWD logs were acquired in the first holes drilled at Site NGHP-01-04 to plan coring and pressure-coring operations in subsequent holes. As Hole NGHP-01-04A was drilled without coring, the LWD data had to be monitored for safety to detect gas entering the wellbore. As explained in the "Downhole Logging" section of the "Methods" chapter, the primary measurement used for gas monitoring was the "annular pressure while drilling" (APWD) measured by the EcoScope tool in the borehole annulus. We looked for sudden decreases of more than 100 psi in the annular pressure, which could be due to low-density gas entering the wellbore. We also monitored pressure increases of the same magnitude, which could be due to fluid acceleration caused by a gas kick (Aldred and others, 1998).

Figure 5 shows the borehole fluid pressure measured in Hole NGHP-01-04A after subtraction of the hydrostatic pressure trend. This residual pressure shows only minor fluctuations that are well below the 100 psi level that would have required preventive action, the only notable features are two pressure spikes of 30–40 psi (at 161 and 186 mbsf) that are likely to be related to drilling (for example, to packing of cuttings in the annulus). We also monitored the coherence of the sonic waveforms acquired by the SonicVISION tool, focusing on the sound velocity in the borehole fluid. Gas indicators would be loss of coherence in the waveforms and a slower sound velocity in the drilling fluid. We found no significant decrease of sonic waveform coherence throughout the interval drilled.

LWD Log Quality

Figure 5 also shows the quality control logs for Hole NGHP-01-04A. The two curves for rate of penetration are an instantaneous rate of penetration (ROPRM) and a rate of penetration averaged over the last 5 feet (ROP5RM). The

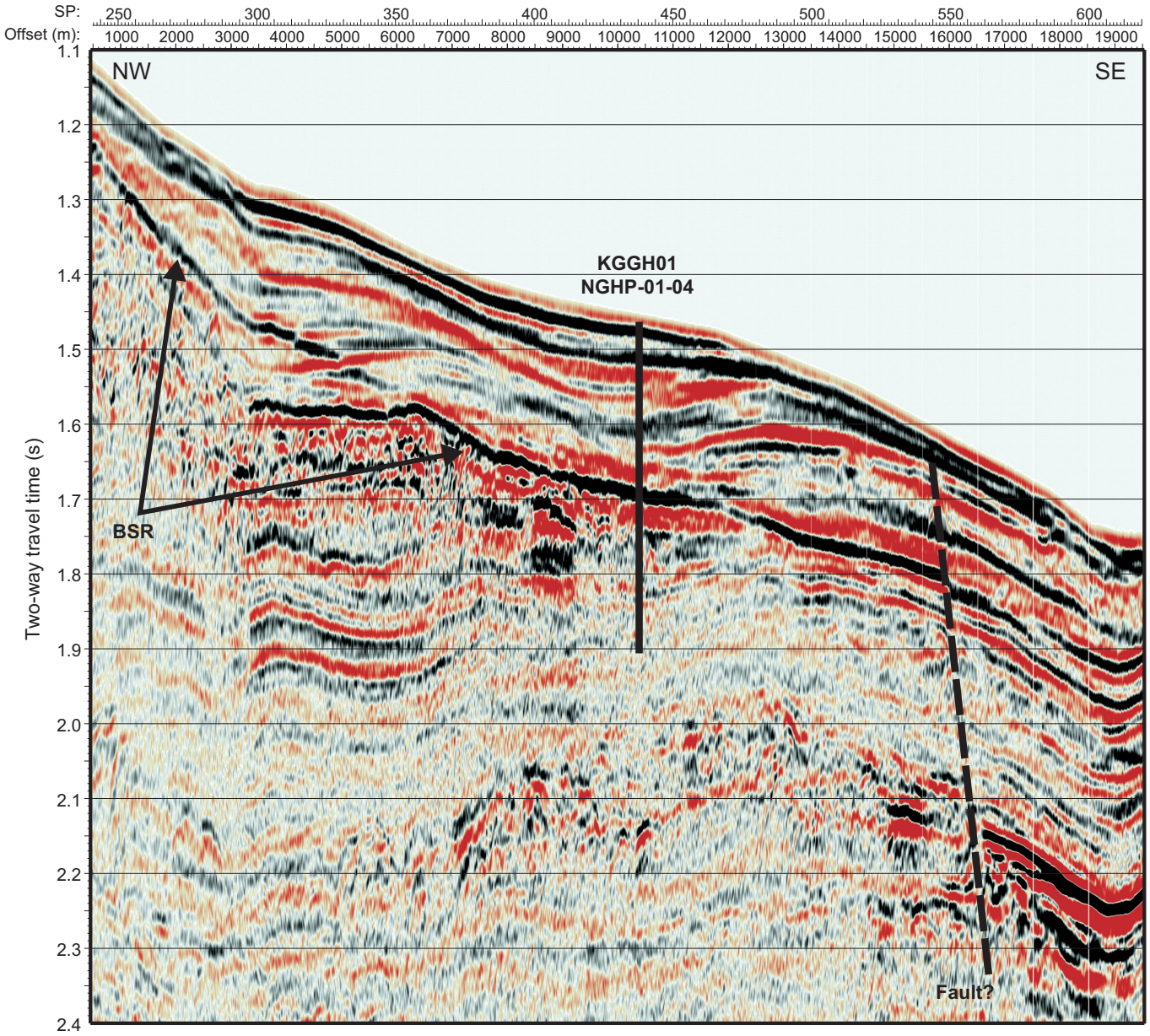

Figure 2. Section of 2D seismic line AD-94-25 around Site NGHP-01-04 (Prospectus Site KGGH01) showing a broad basin and an extensive BSR occurrence. Note the SE-dipping fault, abruptly ending the BSR extent along the line near shot point 550. [BSR, bottom-simulating reflector]

occasional large peaks in the instantaneous rate of penetration are artifacts due to depth fluctuations during pipe connections. The average ROP was about 20 m/h, which was sufficient to record high-resolution GeoVISION resistivity images (for details, see "Downhole Logging" in the "Methods" chapter).

The density (DCAV) and ultrasonic caliper logs (UCAV) show an average borehole diameter that is around 12 in at 40 mbsf and decreases to about 10 in below 110 mbsf. The bit size (dashed line in fig. 5) is 9 7/8 in, and most of the borehole below 110 mbsf is in gauge. The density correction, calculated from the difference between the short-and long-spaced density measurements, is everywhere within the interval 0–0.2 g/cm^3 (fig. 5), suggesting that the density measurements should be of good quality.

Figure 6 is a summary of the LWD gamma ray, density, neutron porosity, and resistivity logs measured in Hole NGHP-01-04A. (SonicVISION results are not shown; they were processed on shore) The gamma ray and resistivity logs measured by the GeoVISION and EcoScope LWD tools generally agree. The GeoVISION and EcoScope gamma ray curves have the same shape, but are offset by about 20–30 gAPI; this difference is most likely due to tool calibration.

Figure 7 shows a comparison of the ring resistivity measured by GeoVISION with the attenuation and phase resistivity curves obtained by the EcoScope tool at different frequencies and coil spacings. For a given coil spacing, the phase-shift EcoScope resistivities have higher vertical resolution than the attenuation resistivities and thus show more detail.

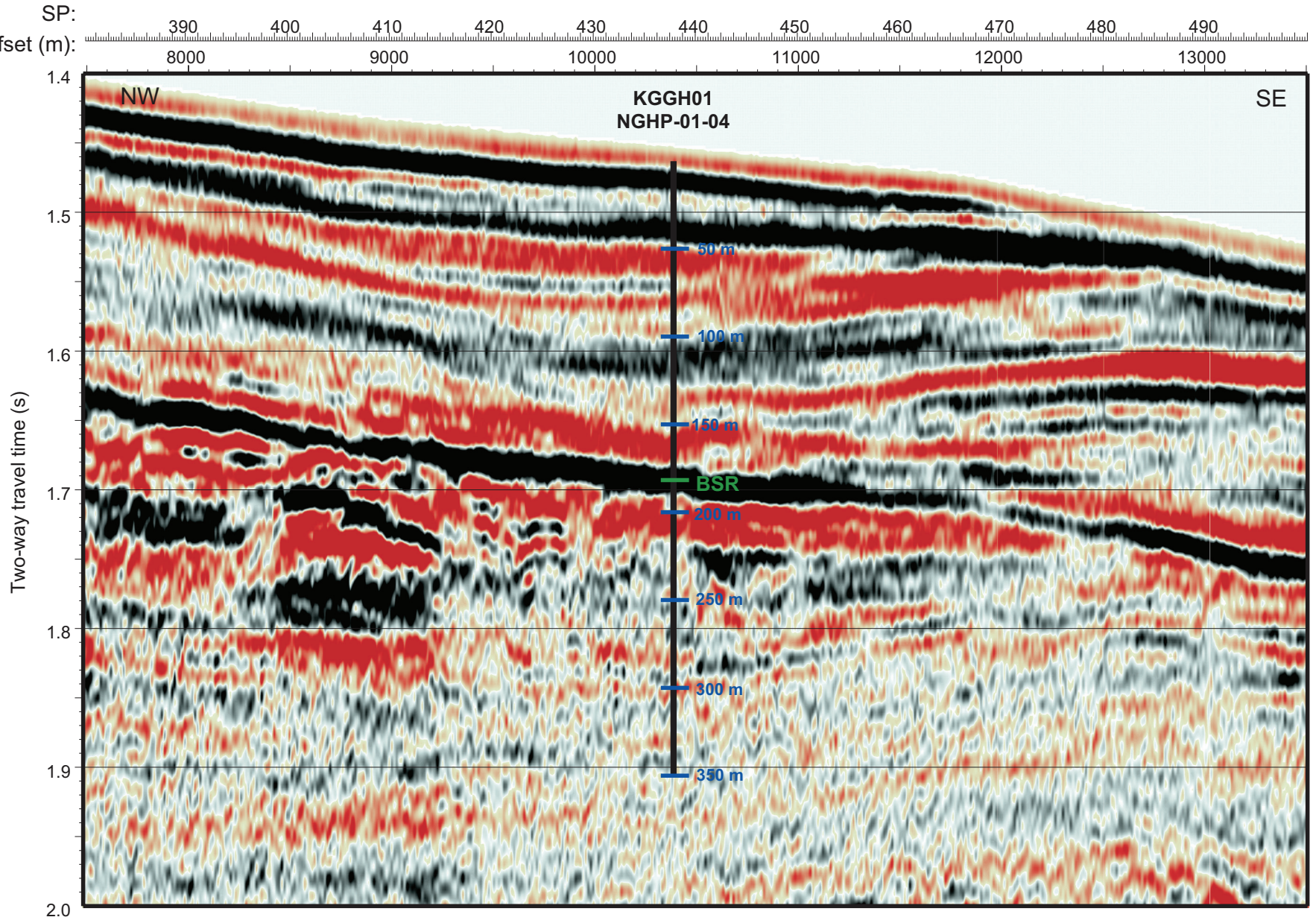

Figure 3. Section of seismic line AD-94-25 around Site NGHP-01-04 (Prospectus Site KGGH01) showing predicted formation tops and BSR depth (~182 mbsf) based on a uniform seismic velocity of 1,580 m/s. [m/s, meters per second]

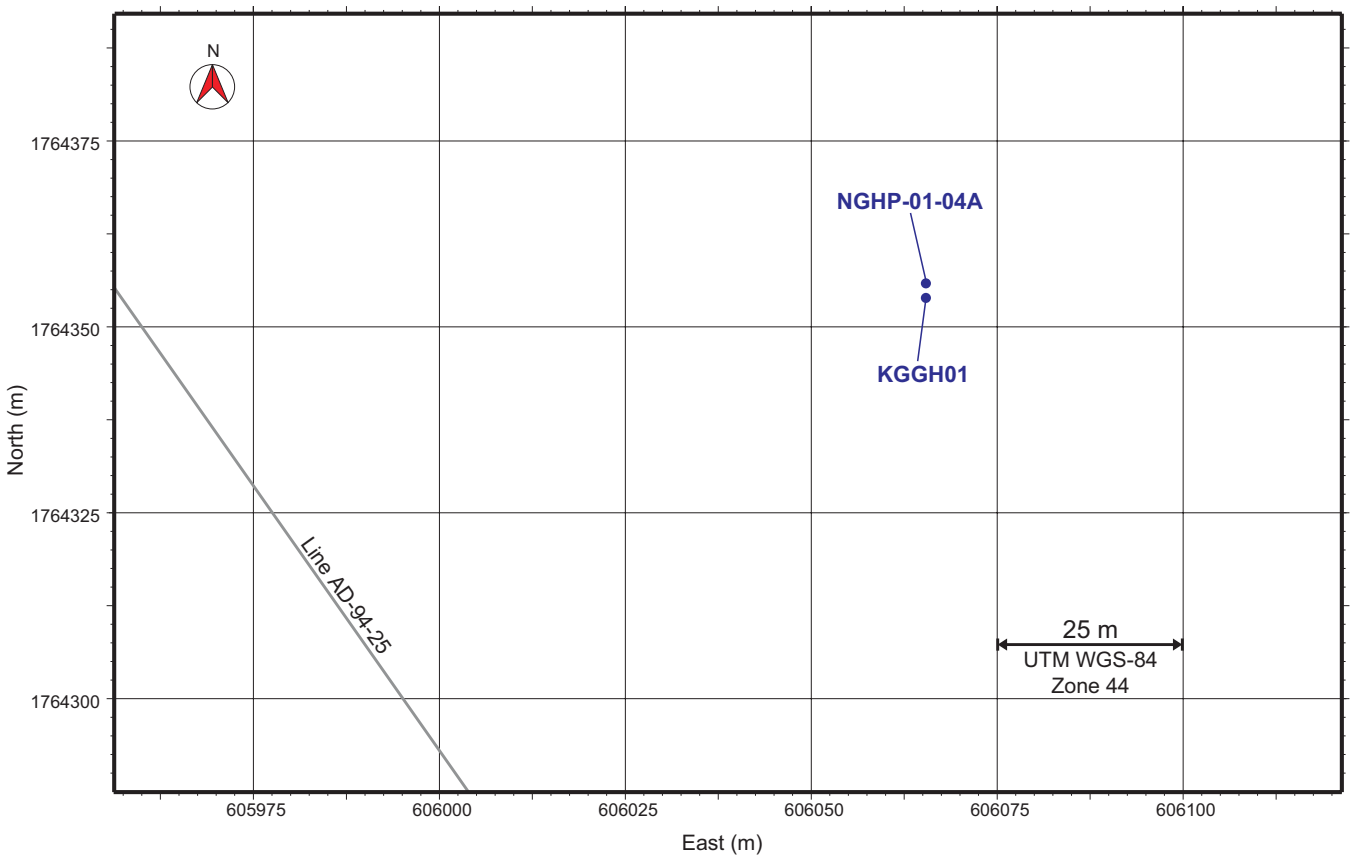

Figure 4. Map showing the hole occupied at Site NGHP-01-04 (KGGH01-A).

A feature of interest in these resistivity curves is the pattern of high and low resistivities in the interval 80–100 mbsf. For any given frequency, as the transmitter-receiver spacing increases, the amplitude of the resistivity high also increases (see especially the phase-shift resistivity curves). Larger transmitter-receiver spacings correspond to greater depths of investigation, and the pattern observed in figure 7 is characteristic of a conductive drilling fluid (in our case, seawater) invading high-resistivity layers that may contain gas hydrates.

Figure 6 also shows two bulk density curves: RHOB is the average density obtained by the EcoScope tool while rotating, while IDRO (image-derived density) is the value of density measured when the sensors were in closest contact with the formation. The two density curves are generally close, except for the interval 36–50 mbsf, where the image-derived density is higher. The measured densities above 110 mbsf, however, may be affected by the hole enlargements shown on the caliper logs (fig. 5).

The bottom-simulating reflector (BSR) that should mark the bottom of the gas-hydrate stability zone was estimated to be at a depth of 182 mbsf in this hole. There is no obvious change in the LWD logs around this depth (fig. 6).

The depths relative to seafloor were fixed for all the LWD logs by identifying the step change in the GeoVISION gamma ray log at the seafloor. For Hole NGHP-01-04A, the gamma ray logging pick for the seafloor was at a depth of 1,083.5 mbrf, 8.5 m above the initial depth estimated by the drillers (1,092 mbrf). The rig floor logging datum was located 10.5 m above sea level.

LWD Porosities

Sediment porosities were calculated from the LWD density and neutron logs in Hole NGHP-01-04A. No core-derived physical property data were available at this site to calibrate and evaluate the log-derived porosities.

The LWD log-derived density measurements (r_b) from Hole NGHP-01-04A were used to calculate sediment porosities (ϕ) with the standard density-porosity relation: $\phi = (\rho_g - \rho_b) / (\rho_g - \rho_w)$. We first used a constant water density (ρ_w) of 1.03 g/cm^3 and a grain/matrix density (ρ_g) equal to 2.72 g/cm^3. The density log-derived porosities from Hole NGHP-01-04A range from about 60 percent at 30 mbsf to about 50 percent at 245 mbsf (fig. 6). The density porosities in figure 6 have been calculated from both the bulk density (RHOB) and the image-derived density curve (IDRO).

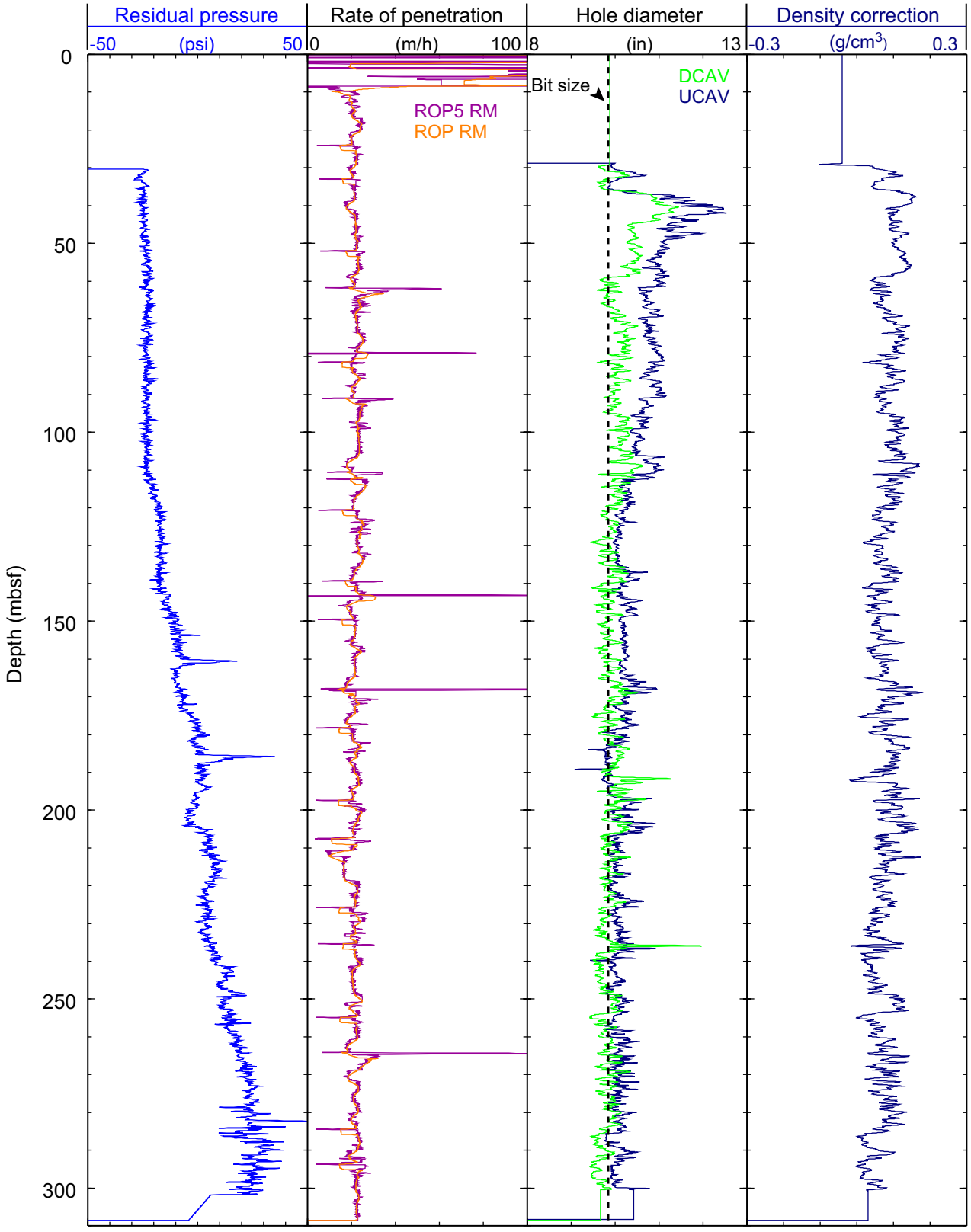

Figure 5. Monitoring and quality control LWD/MWD logs from Hole NGHP-01-04A. [LWD/MWD, logging-while-drilling/measurement-while-drilling; ROPRM, Instantaneous rate of penetration; ROP5RM, Rate of penetration averaged over a 5-ft interval; UCAV, Ultrasonic caliper; DCAV, Density caliper]

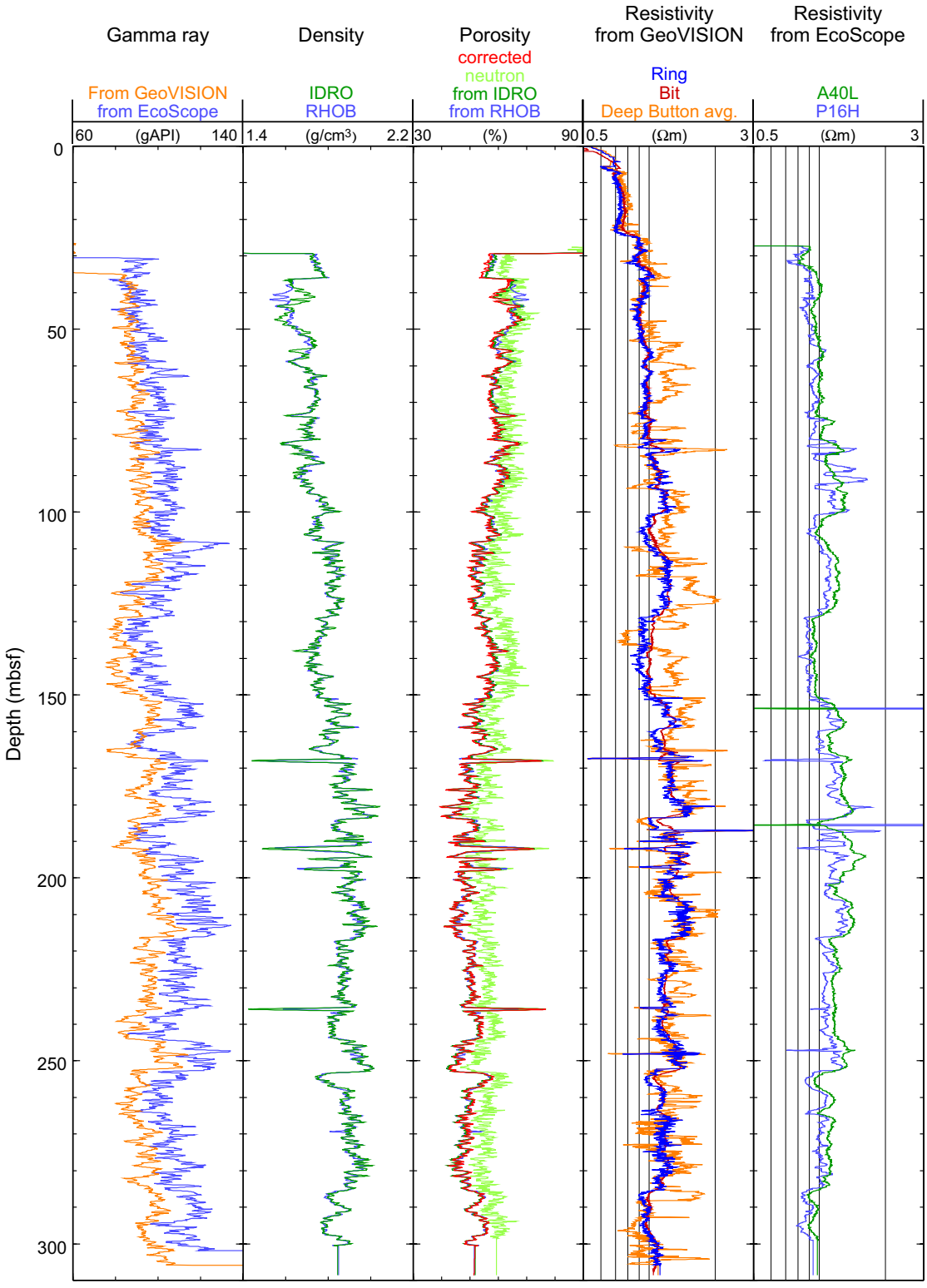

Figure 6. Summary of LWD log data from Hole NGHP-01-04A. [LWD, logging-while-drilling; gAPI, American Petroleum Institute gamma ray units; IDRO, Image-derived density (EcoScope); RHOB, Bulk density (EcoScope); neutron, Thermal neutron porosity (EcoScope); corrected, density porosity with core derived grain densities (EcoScope); RING, Ring resistivity (GeoVISION); BIT, Bit resistivity (GeoVISION); Deep Button avg., Button deep resistivity (GeoVISION); A40L, Attenuation resistivity measured at 400 kHz and a transmitter-receiver spacing of 40 in (EcoScope); and P16H, Phase-shift resistivity at 2 MHZ and a transmitter-receiver spacing of 16 in (EcoScope)]

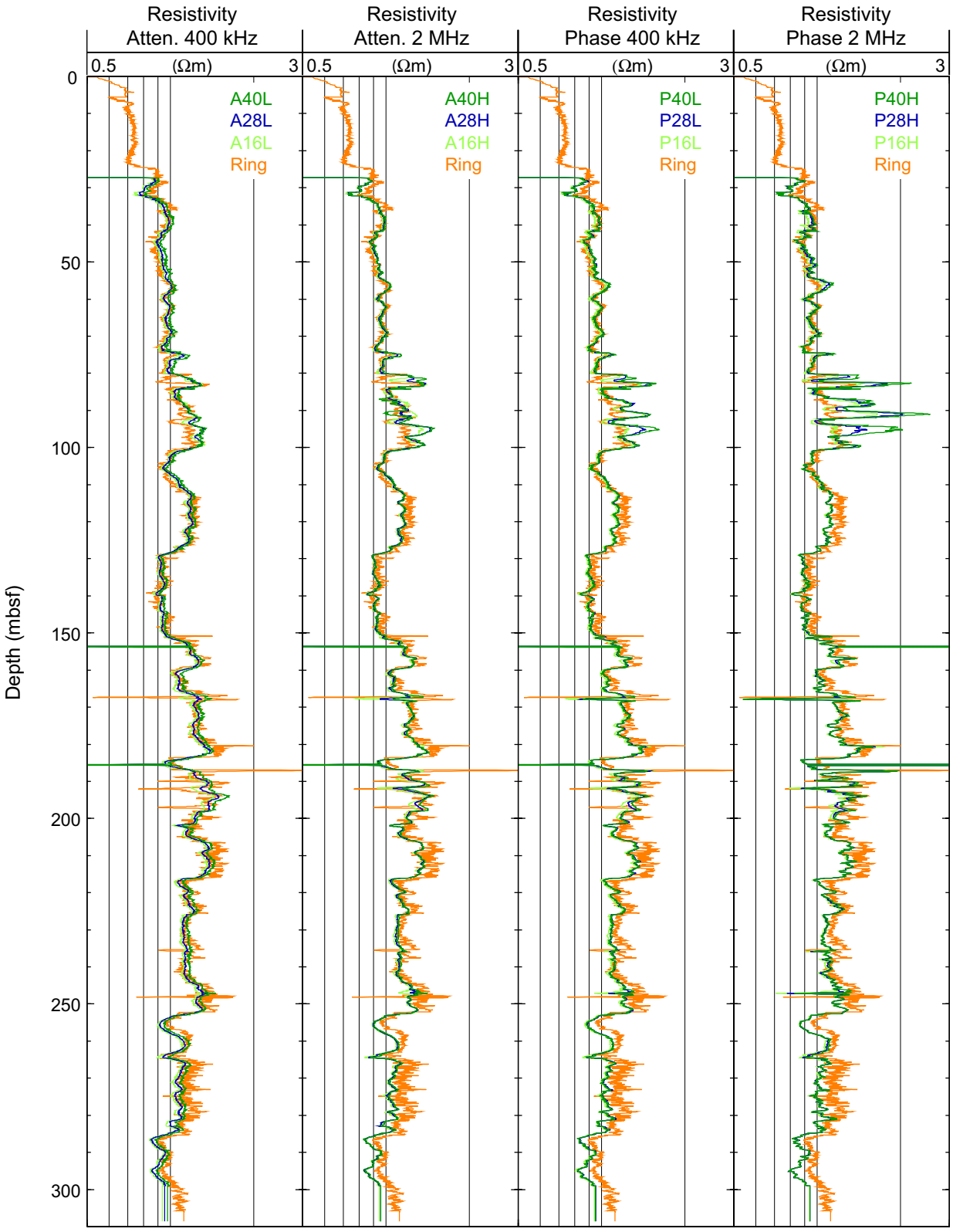

Figure 7. Comparison of LWD resistivity curves from Hole NGHP-01-04A. [LWD, logging-while-drilling; Ring, Ring resistivity (GeoVISION); AXXL, Attenuation resistivity measured at a frequency of 400 kHz, where XX is the transmitter-receiver spacing in inches (EcoScope); AXXH, Attenuation resistivity measured at a frequency of 2 MHz, where XX is the transmitter-receiver spacing in inches (EcoScope); PXXL, Phase-shift resistivity measured at a frequency of 400 kHz, where XX is the transmitter-receiver spacing in inches (EcoScope); PXXH, Phase-shift resistivity measured at a frequency of 2 MHz, where XX is the transmitter-receiver spacing in inches (EcoScope)]

In order to estimate the influence of variable grain density, but without any core sample measurements available at this site, we calculated a "corrected porosity" from the IDRO density log using a least square fourth order polynomial fit with depth of the grain density measurements made on samples from nearby Sites NGHP-01-03 and NGHP-01-05. The results show now discernible difference from the original density porosity derived with constant grain density.

The LWD neutron porosity log from Hole NGHP-01-04A (fig. 6) yielded porosities ranging from an average value near the seafloor of about 60 percent at 30 mbsf to about 55 percent at 300 mbsf. Porosities measured by the neutron log are expected to be higher than those computed from the density log in clay-rich sediments because the neutron log essentially quantifies hydrogen abundance and counts hydrogen in clay minerals as porosity. The neutron porosity measured by the EcoScope tool shown in figure 6 is the "best thermal neutron porosity" (BPHI); it has been corrected so that the effect of clay is reduced (Adolph and others, 2005), and it is only marginally higher than the density porosity.

LWD Borehole Images

The GeoVISION and EcoScope LWD tools generate high-resolution images of borehole log data. The EcoScope tool produces images of density and hole radius (computed on the basis of the density correction, which depends on the borehole standoff). The GeoVISION produces gamma ray and resistivity images with shallow, medium, and deep depth of investigation.

Figure 8 shows some of the LWD images collected by the EcoScope and GeoVISION tools. It should be noted that the display in figure 8 is highly compressed in the vertical direction. The unwrapped images are about 80 cm wide (for a 10 in diameter borehole) and the vertical scale is compressed relative to the horizontal by a factor of about 55:1. These images can be used for detailed sedimentological and structural interpretations and to image gas-hydrate distribution in sediments (for example, in layers, nodules, fractures). Gas-hydrate-bearing sediments exhibit high resistivities within intervals of uniform or low bulk density. Layers with high resistivities and high densities are likely to be low porosity, compacted, or carbonate-rich sediments. The two resistivity images in figure 8 correspond to two depths of investigation (for details, see "Downhole Logging" in the "Methods" chapter).

The main features of interest in the borehole images are the set of high-resistivity macroscopic occurrences in the interval 80–100 mbsf and the single one at ~157 mbsf. These features do not correspond to high densities in the density image and thus may be local gas-hydrate accumulations. As expected, the apparent size of the accumulations increases from shallow to deep resistivity. This is the same pattern observed earlier in the EcoScope resistivities (fig. 7).

Gas Hydrate and Free Gas Occurrence

As previously discussed (see "Downhole Logging" in the "Methods" chapter), the presence of gas hydrate is generally characterized by increases in electrical resistivity and acoustic velocity that are not accompanied by a corresponding porosity decrease. A decrease in porosity alone in water-saturated sediments can result in an increase in resistivity and acoustic velocity. Resistivities logged in Hole NGHP-01-04A show a general negative correlation with porosity (fig. 6), suggesting that little or no gas hydrate is present.

To make a quantitative estimate of the amount of gas hydrate at Site NGHP-01-04, we followed the procedure described in "Downhole Logging" in the "Methods" chapter, to apply the Archie relationship to the resistivity and porosity logs recorded in Hole NGHP-01-04A.

The procedure and the results are shown in figure 5. The pore fluid resistivity (R_w) was estimated from Fofonoff (1985) using a linear temperature profile derived from the *in situ* temperature measurements at nearby Sites NGHP-01-03 and NGHP-01-05 (6.7 °C at the seafloor; gradient of 42 °C/km) and a water salinity defined by a least square polynomial fit with depth of the values measured on pore water samples from Sites NGHP-01-03 and NGHP-01-05 (see "Site NGHP-01-03" and "Site NGHP-01-05" chapters). The estimated m curve is derived from R_w, the porosity (ϕ) and resistivity (R_t) logs ($m_{est} = -\log F / \log \phi$, where $F = R_t / R_w$). As this relationship is defined for water-saturated sediments, the chosen value of $m = 2.1$ is given by the baseline of this curve in the low-resistivity intervals where there is likely no gas hydrate. Using the porosity log and Archie's equation ($R_0 = (a\, R_w) / \phi^m$), we derive the predicted resistivity of the water-saturated formation R_o. A qualitative influence of gas hydrate on the resistivity log is indicated by the difference between the R_0 and the measured resistivity R_t. The estimated water saturation, assumed to be the numerical complement of the hydrate saturation, is $S_w = (R_0/R_t)^{1/n}$, where n=2 (Pearson and others, 1983). We used the "corrected" density porosity computed from the image-derived density (IDRO) and the resistivity from the 16 in, phase-shift, high-frequency propagation resistivity (P16H) measured by the EcoScope tool. We use the P16H curve because it is the resistivity with the highest vertical resolution measured by the EcoScope.

As noted earlier, porosity and resistivity curves in Hole NGHP-01-04A generally mirror each other, so that the computed water-saturated resistivity R_0 is very close to the measured resistivity R_t and the water saturation S_w is close to 100 percent throughout most of the logged interval (fig. 9). The only exceptions where the computed S_w is less than 100 percent are in the intervals 53–61 mbsf and 80–100 mbsf. The shallower interval corresponds to a low in measured density, and thus may be due to an underestimation of density in the shallow enlarged part of the hole (see the caliper in fig. 5).

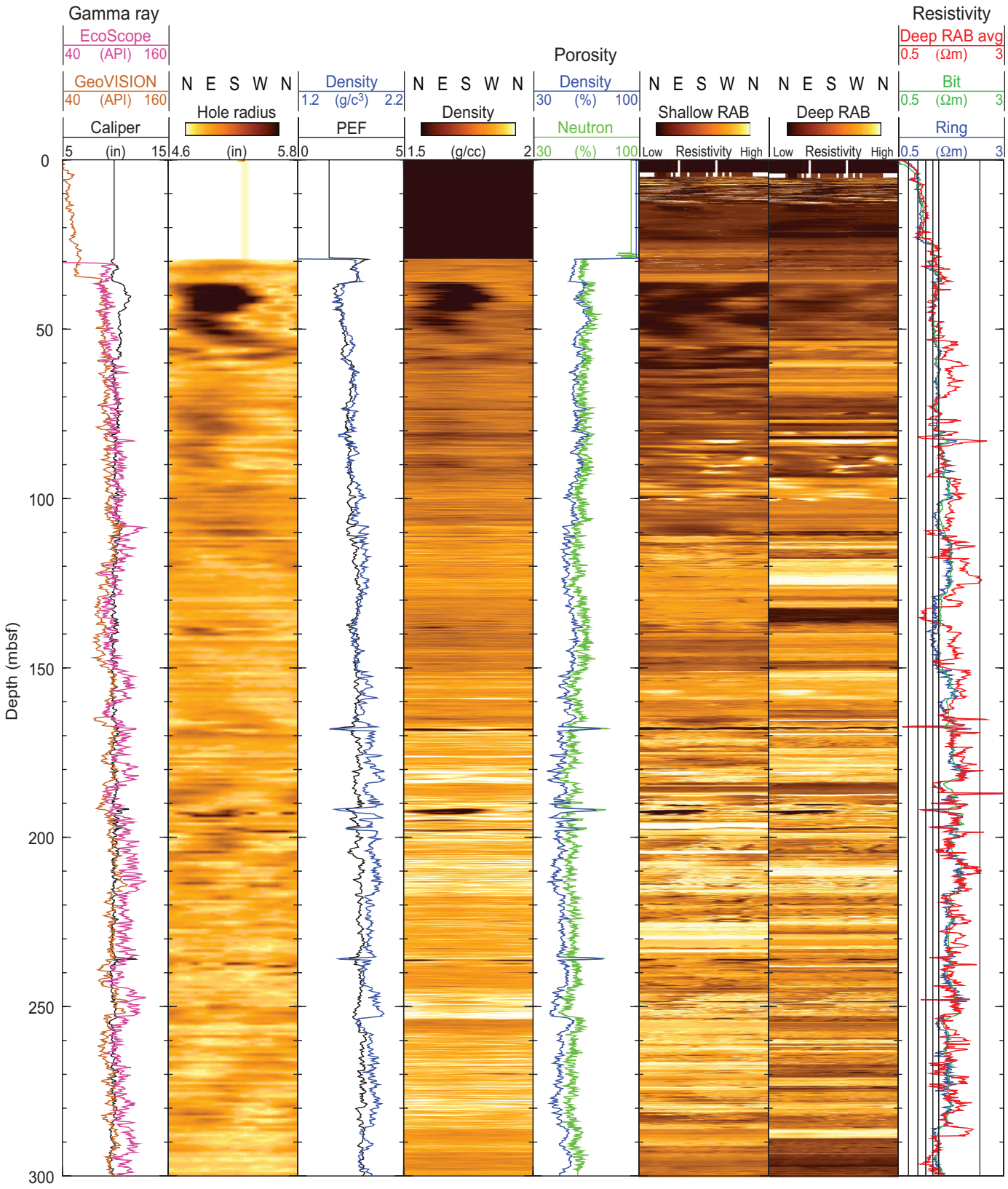

Figure 8. LWD image data from Hole NGHP-01-04A. [LWD, logging-while-drilling; gAPI, American Petroleum Institute gamma ray units; RAB, Resistivity-At-Bit image obtained by the GeoVISION tool]

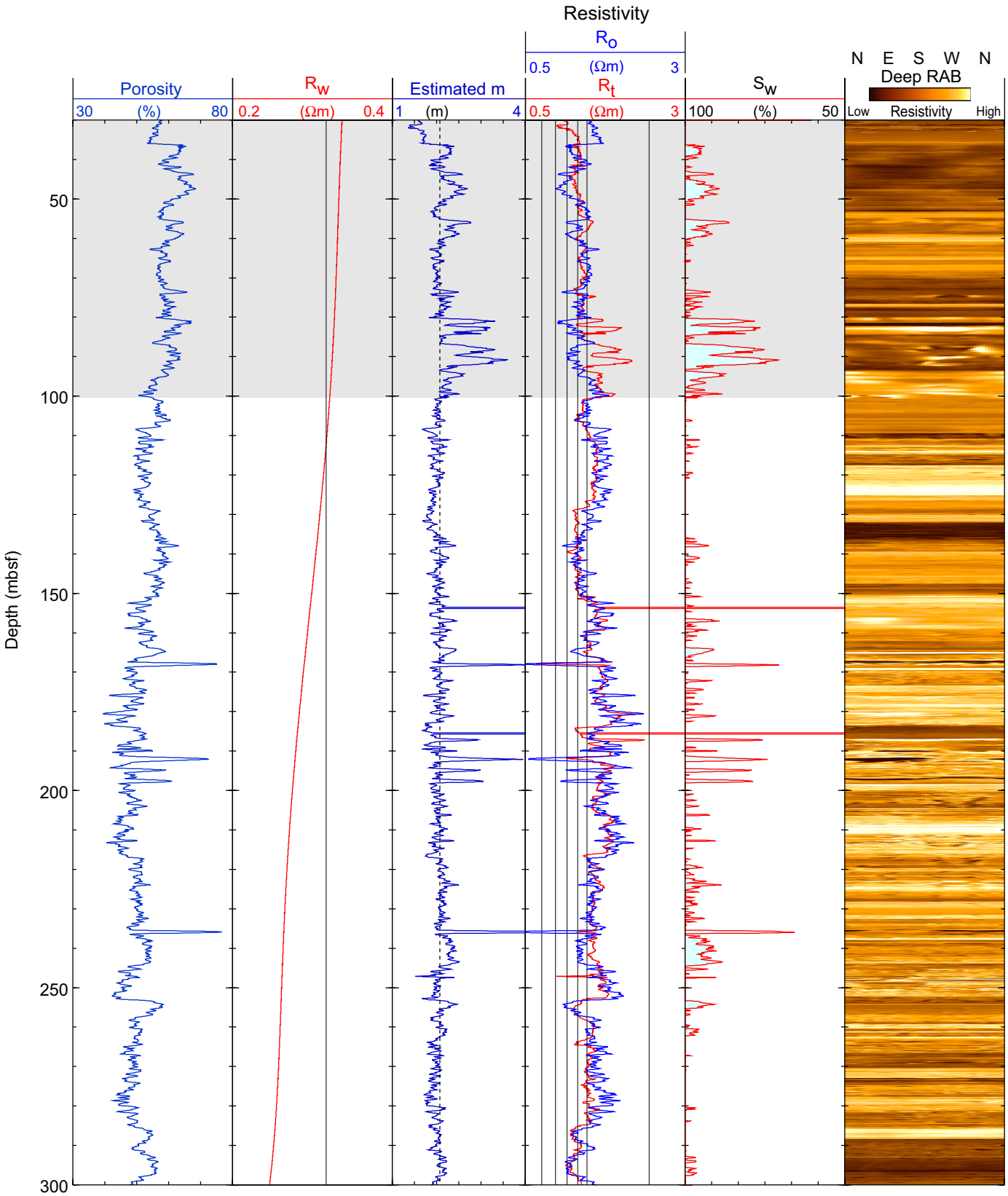

Figure 9. Water saturations from Archie's equation and LWD porosity and resistivity logs in Hole NGHP-01-04A. The gray area indicates degraded data quality. [LWD, logging-while-drilling; R_w, formation water resistivity; R_0, computed formation resistivity for 100 percent water saturation; R_t, measured resistivity; S_w, water saturation]

On the other hand, the interval 80–100 mbsf is more likely to contain gas hydrate because it corresponds to a resistivity high because the EcoScope resistivities suggest invasion of conductive drilling fluid in a resistive formation (fig. 7), and because the resistivity images show high-resistivity macroscopic occurrences (fig. 8).

References Cited

Adolph, B., Archer, M., Codazzi, D., el-Halawani, T., Perciot, P., Weller, G., Evans, M., Grant, J., Griffiths, R., Hartman, D., Sirkin, G., Ichikawa, M., Scott, G., Tribe, I., and White, D., 2005, No more waiting—Formation evaluation while drilling: Oilfield Review, Autumn 2005, p. 4–21.

Aldred, W., Cook, J., Bern, P., Carpenter, B., Hutchinson, M., Lovell, J., Rezmer-Cooper, I., and Leder, P.C., 1998, Using downhole annular pressure measurements to improve drilling performance: Oilfield Review, Winter 1998, p. 40–55.

Fofonoff, N.P., 1985, Physical properties of seawater: Journal of Geophysical Research, v. 90, no. C2, p. 3332–3342.

Pearson, C.F., Halleck, P.M., McGuire, P.L., Hermes, R., and Mathews, M., 1983, Natural gas hydrate deposits—A review of *in situ* properties: Journal of Physical Chemistry, v. 87, p. 4180–4185.